Hydroelastic vibration analysis of plates partially submerged in fluid with an isogeometric FE-BE approach

M. Erden Yildizdag[a,*], I. Tugrul Ardic[b], Murat Demirtas[c], Ahmet Ergin[b]

[a] *Department of Mechanical Engineering, University of California, Berkeley, CA, 94720, USA*
[b] *Faculty of Naval Architecture and Ocean Engineering, Istanbul Technical University, Maslak, 34469, Istanbul, Turkey*
[c] *Turkish Airlines General Management Building Ataturk Airport, Yesilkoy, 34149, Istanbul, Turkey*

Abstract

The hydroelastic vibration analysis of clamped rectangular plates both vertically and horizontally submerged in fluid is studied by isogeometric FE/BE approach in this paper. By adopting the linear hydroelasticity theory, the computational procedure of the fluid-structure interaction problem is divided into two parts. In the first part, dynamic analysis of the structure in vacuo conditions and in the absence of external forces is carried out by NURBS-based isogeometric finite element method (IGAFEM). Then, in the second part, it is assumed that fluid is inviscid, incompressible and irrotational, and fluid forces directly correspond to inertial effects of the structure. Thus, displacements of the elastic structure due to modal vibrations are in same phase with the acceleration of the fluid particles, and fluid forces on the freely vibrating structure are obtained by NURBS-based isogeometric boundary element method (IGABEM). In order to verify the accuracy of the present methodology, a convergence study is carried out with the available numerical and experimental data providing the generalized added mass coefficients, and the effects of the thickness and aspect ratio are also investigated. It is found that the numerical results are in good agreement

*Corresponding author
Email address: yildizdag@berkeley.edu (M. Erden Yildizdag)

with the previous results, thus validating the proposed approach.

Keywords: isogeometric analysis, hydroelasticity, finite element method, boundary element method

2010 MSC: 00-01, 99-00

1. Introduction

The dynamic behavior of structures in contact with fluid must be accurately determined for performing its task securely while it is being used within a specific purpose. A velocity potential is induced in the fluid medium due to transmission of structural vibrations into the fluid, and this leads to an increase in the kinetic energy of the system. This phenomenon results in the dynamic characteristics of the structure in contact with fluid differing significantly from those exposed only to air. It is therefore very important to have an accurate understanding of the dynamic interaction effects of the coupled fluid-structure system in order to design engineering structures. As a structural component, curved and flat plates are commonly used in many engineering fields such as aviation, marine engineering, nuclear power plants, and the petrochemical industry. In shipbuilding and offshore engineering, plates are typically used as side plating of hulls, protuberances, rudders, and tank bulkheads.

In the past half century, various studies have been conducted to compute the hydroelastic vibration characteristics of plates. The effects of fluid loading on vibrating rectangular plates were first studied by Lindholm et al. (1965). In their study, hydroelastic vibration characteristics of both partially and fully submerged rectangular plates were investigated via experiments. Meyerhoff (1970) modeled fluid motions by dipole singularities, and then calculated added mass coefficients for thin rectangular plates. Implementation of the finite element method for hydroelastic vibration problems has been initiated by Zienkiewicz and Newton (1969), Marcus (1978) and Muthuveerappan et al. (1979), by modeling the surrounding fluid with finite elements to solve the pressure field around the structure. Fu and Price (1987) applied the linear hydroelasticity theory by

using the boundary element method to predict the dynamic characteristics of both vertical and horizontal surface-piercing plates including the effects of free surface waves. Kwak (1996) applied the Rayleigh-Ritz method in conjunction with the boundary element method to obtain non-dimensionalized added virtual mass incremental (NAVMI) factor for simply supported and clamped plates considering free surface and rigid wall conditions. Liang et al. (2001) utilized the empirical added mass formulation to calculate the hydrodynamic vibration characteristics of submerged cantilever plates. The boundary element method in conjunction with the image method to perform the infinite frequency limit on the free surface was first applied by Ergin and Uğurlu (2003). Kerboua et al. (2008) adopted a finite element method framework in conjunction with Sander's shell theory to analyze plate structures. In their study, both plates floating on a free surface and submerged in fluid under different boundary conditions are considered, and it is observed that the hybrid approach combining Sander's shell theory and finite element technique is more precise than conventional finite element methodologies. Hashemi et al. (2012, 2010) studied relatively thick plates by employing Mindlin plate theory with the Rayleigh-Ritz method. In Hashemi et al. (2010), rectangular plates resting on a Pasternak foundation were studied, and the results were compared with the numerical results presented by Zhou and Cheung (2000) and Uğurlu et al. (2008).

Besides the aforementioned rectangular plates, plates reinforced by deep or slender stiffeners are widely used in ship and submarine structures to increase stiffness and avoid resonant vibrations. Li et al. (2011) studied hydroelastic vibrations of stiffened bottom plates of fluid tanks through analytical procedures and noticed the phenomenon of "mode reversal" that implies the reversal of the first two mode shapes of stiffened plates in contact with air and water. Cho et al. (2014) studied vibration characteristics of vertical stiffened plates by combining strain and kinetic energy expressions of stiffeners and plate. In their study, the potential flow theory assumptions were adopted ignoring the free surface waves, and the displacement components of the stiffened plate were obtained by using Timoshenko beam functions in conjunction with the Mindlin plate theory.

In recent studies, several authors have taken an interest in hydroelastic vibration characteristics of composite plates and active vibration control of structures under fluid-structure interaction, as well as effects of compressibility of the fluid on the dynamic characteristics of the plates. Kwak and Yang (2013) studied the flexural vibrations of cantilever plate partially submerged into fluid by utilizing elliptical coordinate system to define the mathematical expression of the dynamically coupled system, and the added virtual mass matrix is combined with the dynamic model of the plate obtained by the Rayleigh-Ritz approach. In the same manner, Kwak and Yang (2015) studied active vibration control of rectangular plates either partially or fully submerged in fluid. In their study, an added virtual mass matrix obtained by using the authors' previous work (Kwak and Yang, 2013) was combined with the dynamic model of the plate. It was also observed a high degree of consistency between theoretical and experimental results, and sufficient damping of the vibrations of the rectangular plate are obtained both in air and water. Canales and Mantari (2017) presented an analytical solution for hydroelastic vibration analysis of thick composite plates by adopting combined higher order shear deformation theory. Liao and Ma (2016) studied the effects of compressibility of the surrounding fluid on the hydroelastic vibration characteristics of the structures.

Although Computer Aided Engineering (CAE) and Computer Aided Design (CAD) have had spectacular progress in the last decades, drawbacks in terms of geometry and data transfer, especially for complex structures, were major bottlenecks until recently. In order to create an analysis-suitable geometry for the use of discretization-based numerical methods, mesh generation is tedious and time-consuming, especially in regions with high curvature which require mesh refinement. The main idea underlying the isogeometric analysis (IGA) is to provide a straightforward and non-adjusting interconnection between CAD and CAE tools that enables reduction in major time-consuming engineering processes such as mesh generation and geometry construction, which span 80% of the overall analysis time (Cottrell et al., 2009). The principles of IGA were first introduced by Hughes et al. (2005) to perform numerical computations with

desirable accuracy even with low mesh density, using the same basis functions both in geometry and analysis with low computational cost. The detailed mathematical theory of IGA was presented by Bazilevs et al. (2006b). In pursuit of these seminal papers, IGA was extensively applied in a wide range of fields such as biomedical engineering (Zhang et al., 2007), fracture mechanics (De Luycker et al., 2011), contact mechanics (Temizer et al., 2011), fluid-structure interaction (Bazilevs et al., 2006a), elastostatics (Simpson et al., 2012), shape optimization (Yoon and Cho, 2016) and structural vibration (Shojaee et al., 2012). Thai et al. (2012) and Luu et al. (2015) studied the vibration problems of laminated plates and curved beams, respectively. Wang et al. (2015) proposed a novel approach by using isogeometric higher order mass matrices possessing 4th- and 6th-order accuracies in the eigenvalue problems. Zhao et al. (2017) applied a multi-patch isogeometric finite element method for free vibration analysis of thick plates. As for the developments in hydrodynamics, Politis et al. (2009) extended the IGA concept to boundary element method to solve 2D exterior Laplace problems. Belibassakis et al. (2013) extended the previous analysis of Politis et al. (2009) to solve the wavemaking resistance problem of surface-piercing 3D geometries. Takahashi and Matsumoto (2012) implicated the fast multiple method (FMM) into the isogeometric boundary element method to deal with 2D large-scale Laplace problems. Recently, Gong and Dong (2017) extended the standard 3D isogeometric boundary element method by employing an adaptive integration for potential problems and indicated that the effectiveness of the adaptive method appears where the lengths of adjacent panels are considerably different.

The hydroelastic vibration analysis of cantilever rectangular plates both vertically and horizontally in contact with fluid is studied with different submergence ratios in this paper. According to the authors' best knowledge, this is the first study to investigate hydroelastic vibration characteristics of plates by employing the versatile IGA concept into both finite element-based in-vacuo structural analysis and boundary element-based potential flow analysis. In addition, it can be emphasized as a result of deep literature review by the authors that there are not any other studies employing the infinite frequency free sur-

face condition by using the image method in conjunction with the isogeometric boundary element method. In this study, fluid-structure interaction effects are obtained by a NURBS-based isogeometric boundary element method. The zero velocity potential on the free surface is applied by using the image method with the assumption that the structure vibrates in the high frequency region. Besides, it is also assumed that the fluid is ideal, and fluid forces are in phase with inertial effects of the surrounding fluid, in other words, the fluid pressure on the wetted surface is associated with the structural acceleration which enables the application of hydroelasticity theory. In this theory, the hydroelastic vibration problem can be divided into two sub-problems, called as "in-vacuo" and "wet" analyses, respectively. The in-vacuo analysis involves determining the dynamic characteristics of the structure by solving the equations of motion in the absence of structural damping and external force. In this study, the Kirchhoff plate theory is applied and material is assumed to be isotropic, and the structural mass and stiffness matrices are formed by employing the isogeometric finite element method (IGAFEM). In the wet analysis, in-vacuo structural displacements obtained by using IGAFEM directly constitute the boundary conditions of the potential problem, and the discretized integral equation of Laplace problem is solved by the isogeometric boundary element method (IGABEM). Fluid-structure interaction effects are represented by the generalized hydrodynamic added mass coefficients. In this study, the computational domain is defined by non-uniform rational b-splines (NURBS) and the isoparametric approach is adopted to obtain source strengths which are also represented by NURBS basis functions. The total mass matrix is obtained by merging the structural mass matrix with the added-mass matrix and the eigenvalue problem is solved for partially or totally submerged cantilever plates.

The organization of the rest of the paper is as follows: a brief review of non-uniform rational b-splines is given in Section 2, then Section 3 details the numerical approach to calculate the hydroelastic vibration characteristics of plates partially or fully submerged into fluid in the context of the isogeometric approach. The numerical implementation of the proposed method is detailed in

Section 4. Finally, in Section 5, cantilever rectangular plates both submerged in vertical and horizontal positions are analyzed with different submergence ratios, and the predicted hydroelastic vibration characteristics are compared with the available experimental and numerical results.

2. Non Uniform Rational B-Splines (NURBS)

Because of its ability to represent geometries more accurately, NURBS becomes a standard tool in CAD systems to design complex objects. Since B-Splines are the progenitors of the NURBS, definition of the B-Splines is an essential starting point on the way to comprehend the NURBS, which is the key structure to implement a IGA framework. In this section, formulation of the NURBS is briefly explained following Piegl and Tiller (1995), Rogers (2000), and Hughes et al. (2005).

In order to create a NURBS patch, three parameters - knot vector(s), control points and weights - have to be defined. A knot vector is the non-decreasing coordinates of the parametric domain, and it is defined in each parametric direction of the NURBS patch. Also, it defines the partition of the parametric domain in the corresponding direction in the form of

$$\Xi = [\xi_1, \xi_2, \ldots, \xi_{n+p+1}] \quad \xi_i \in \mathbb{R}, \tag{1}$$

where i is the knot index, $i = 1, 2, ..., n + p + 1$, p is the polynomial order, and n is the number of basis functions which comprise the B-Spline. Control points are defined as vector valued coefficients of the basis functions in order to control the shape of the patch, and weights are assigned to reflect how much the particular control point affects the curve. A pth-order 1-D NURBS patch (curve), therefore, may be expressed as follows

$$\boldsymbol{C}(\xi) = \sum_{i=1}^{n} R_i^p(\xi)\boldsymbol{P}_i, \tag{2}$$

where $R_i^p(\xi)$ is the pth-order rational basis function defined by

$$R_i^p(\xi) = \frac{N_{i,p}(\xi)w_i}{\sum_{\hat{j}=1}^{n} N_{\hat{j},p}(\xi)w_{\hat{j}}}, \tag{3}$$

$\boldsymbol{P}_i$ is the coordinates of the ith control point, w_i is the weight of the ith control point, and $N_{i,p}$ is the pth-order B-spline basis function given as follows for $p = 0$,

$$N_{i,0}(\xi) = \begin{cases} 1 & \text{if } \xi_i \leq \xi \leq \xi_{i+1}, \\ 0 & \text{otherwise,} \end{cases}$$

and for $p = 1, 2, 3, ...,$

$$N_{i,p}(\xi) = \frac{\xi - \xi_i}{\xi_{i+p} - \xi_i} N_{i,p-1}(\xi) + \frac{\xi_{i+p+1} - \xi}{\xi_{i+p+1} - \xi_{i+1}} N_{i+1,p-1}(\xi). \tag{4}$$

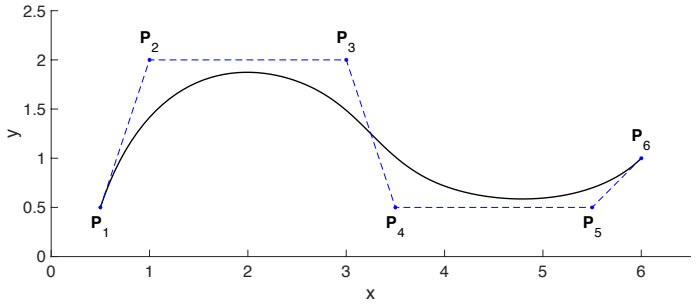

Figure 1: NURBS curve with knot vector Ξ=[0, 0, 0, 0, $\frac{1}{3}$, $\frac{2}{3}$, 1, 1, 1, 1] and uniform weights

A 3rd-order NURBS curve and its B-spline basis functions are depicted in Figs. 1 and 2, respectively.

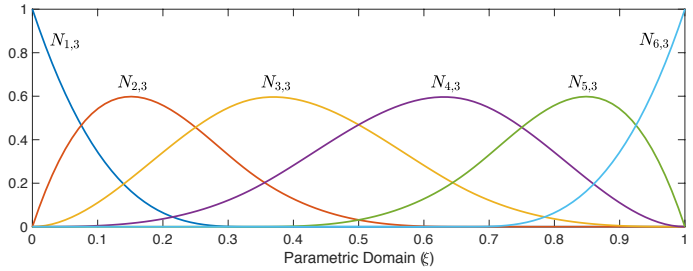

Figure 2: 1-D B-Spline basis functions of knot vector Ξ=[0, 0, 0, 0, $\frac{1}{3}$, $\frac{2}{3}$, 1, 1, 1, 1]

Likewise, NURBS surfaces are defined as follows

$$\boldsymbol{S}(\xi, \eta) = \sum_{i=1}^{n} \sum_{j=1}^{m} R_{i,j}^{p,q}(\xi, \eta) \boldsymbol{P}_{i,j}, \tag{5}$$

where

$$R_{i,j}^{p,q} = \frac{N_{i,p}(\xi)M_{j,q}(\eta)w_{i,j}}{\sum_{\hat{i}=1}^{n}\sum_{\hat{j}=1}^{m}N_{\hat{i},p}(\xi)M_{\hat{j},q}(\eta)w_{\hat{i},\hat{j}}} \tag{6}$$

is the 2-D rational basis functions, $\boldsymbol{P}_{i,j}$ is the control points (control net). Here, $N_{i,p}$ and $M_{j,q}$ are pth and qth order b-spline basis functions defined with knot vectors $\Xi = [\xi_1, \xi_2, \ldots, \xi_{n+p+1}]$ and $\mathcal{H} = [\eta_1, \eta_2, \ldots, \eta_{m+q+1}]$. Also, n and m are the number of basis functions in each parametric direction ξ and η, respectively. In this study, all the spline and IGA connectivity algorithms have been implemented following Piegl and Tiller (1995) and Cottrell et al. (2009).

3. Mathematical Model

3.1. In-vacuo Analysis

In this part, we present the mathematical model of the in-vacuo analysis which consists of the formulation of the free vibration analysis for thin plates. In order to formulate the problem, we consider a plate on a right-handed Cartesian coordinate system with the thickness t in z direction (Fig. 3).

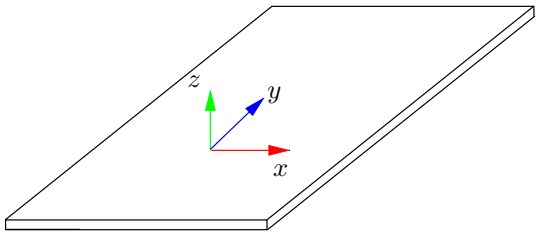

Figure 3: Plate geometry

Based on the Kirchhoff plate theory, it is assumed that a line normal to the midplane remains normal after the deformation, the normal stress σ_{zz} is negligible, the thickness does not change during the deformation, and the points on the mid-plane move only in the vertical direction. Therefore, the displacement field is expressed as follows

$$\mathbf{u} = -z\frac{\partial w}{\partial x}\,\mathbf{i} - z\frac{\partial w}{\partial y}\,\mathbf{j} + w\,\mathbf{k}, \tag{7}$$

where w is the deflection in z direction, and it is the only independent variable in the problem. Then, the infinitesimal strain tensor reads

$$\begin{aligned}
\varepsilon_{xx} &= u_{x,x} = -z\frac{\partial^2 w}{\partial^2 x},\\
\varepsilon_{yy} &= u_{y,y} = -z\frac{\partial^2 w}{\partial^2 y},\\
\varepsilon_{xy} &= \frac{1}{2}\left(u_{x,y} + u_{y,x}\right) = -z\frac{\partial^2 w}{\partial x \partial y},\\
\varepsilon_{xz} &= \varepsilon_{yz} = \varepsilon_{zz} = 0.
\end{aligned}$$

The displacement field and the infinitesimal strain tensor are inserted into the weak form of the free vibration problem,

$$\int_{\Omega} \delta\boldsymbol{\varepsilon} \cdot \boldsymbol{\sigma}(\mathbf{u})\, d\Omega + \int_{\Omega} \rho\, \delta\mathbf{u} \cdot \ddot{\mathbf{u}}\, d\Omega = 0, \tag{8}$$

and by substituting suitable approximations with rational basis functions,

$$w = \sum_{i=1}^{n}\sum_{j=1}^{m} R_{i,j}^{p,q}\, w_{i,j}, \quad \delta w = \sum_{i=1}^{n}\sum_{j=1}^{m} R_{i,j}^{p,q}\, \delta w_{i,j}, \tag{9}$$

and integrating over the thickness (in z direction), the following system of equations is obtained (by imposing the condition is valid for every δw)

$$[\mathbf{M}]\{\ddot{\mathbf{w}}\} + [\mathbf{K}]\{\mathbf{w}\} = \mathbf{0}, \tag{10}$$

where $[\mathbf{M}]$ and $[\mathbf{K}]$ are the global mass and stiffness matrices, respectively. In IGAFEM procedure, these matrices are assembled calculating the local stiffness matrix,

$$[\mathbf{K}^e] = \int_{\Omega^e} [\mathbf{B}^e]^T [\mathbf{D}] [\mathbf{B}^e]\, d\Omega^e \tag{11}$$

where

$$[\mathbf{B}^e] = \begin{bmatrix} B_{1,1}^e & B_{2,1}^e & \ldots & B_{p+1,q+1}^e \end{bmatrix}, \quad B_{i,j}^e = \begin{bmatrix} \frac{\partial^2 R_{i,j}^e}{\partial^2 x} \\ \frac{\partial^2 R_{i,j}^e}{\partial^2 y} \\ \frac{\partial^2 R_{i,j}^e}{\partial x \partial y} \end{bmatrix}, \tag{12}$$

and the local mass matrix,

$$[\mathbf{M}^e] = \int_{\Omega^e} \left(\rho t \, [\mathbf{N}_1^e]^T [\mathbf{N}_1^e] + \rho \frac{t^3}{12} \, [\mathbf{N}_2^e]^T [\mathbf{N}_2^e] \right) d\Omega^e \tag{13}$$

where

$$[\mathbf{N}_1^e] = \begin{bmatrix} R_{1,1}^e & R_{2,1}^e & \dots & R_{p+1,q+1}^e \end{bmatrix} \tag{14}$$

and

$$[\mathbf{N}_2^e] = \begin{bmatrix} \frac{\partial R_{1,1}^e}{\partial x} & \frac{\partial R_{2,1}^e}{\partial x} & \dots & \frac{\partial R_{p+1,q+1}^e}{\partial x} \\ \frac{\partial R_{1,1}^e}{\partial y} & \frac{\partial R_{2,1}^e}{\partial y} & \dots & \frac{\partial R_{p+1,q+1}^e}{\partial y} \end{bmatrix}, \tag{15}$$

over the each finite element, and $R_{i,j}^e$ represents the non-zero rational basis functions within the corresponding element, Ω^e. Also, for linear isotropic materials, the elasticity tensor takes the following matrix form

$$[\mathbf{D}] = \frac{Et^3}{12(1-\nu^2)} \begin{bmatrix} 1 & \nu & 0 \\ \nu & 1 & 0 \\ 0 & 0 & 1-\nu \end{bmatrix}, \tag{16}$$

where E and ν are the Young's modulus and the Poisson's ratio, respectively. By solving the formulated eigenvalue problem Eq. (10), the in-vacuo natural frequencies and corresponding mode shapes are obtained to be used in the wet analysis.

3.2. Wet Analysis

When the fluid is assumed ideal, i.e. inviscid and incompressible, and its motion is irrotational, there exist a fluid velocity vector due to structural vibrations, $\mathbf{v}$, which defined as the gradient of the velocity potential function Φ as

$$\mathbf{v}(x, y, z, t) = \nabla \Phi(x, y, z, t), \tag{17}$$

where

$$\Phi(x, y, z, t) = \sum_{j=1}^{M} \mathrm{Re}\left[i\omega \phi_j(x, y, z) \mathrm{e}^{i\omega t} \right], \tag{18}$$

and ϕ_j satisfies the Laplace's equation, $\nabla^2\phi(x,y,z) = 0$, throughout the fluid domain. On the wetted surface of the structure, the kinematic boundary condition is appropriate. This condition implies that the surface normal component of the fluid velocity must be equal to the normal velocity of the boundary surface due to the modal vibrations and it can be defined as

$$\frac{\partial \phi_r}{\partial n} = -\mathbf{u}_r \cdot \mathbf{n}, \tag{19}$$

where $\mathbf{u}_r$ corresponds to the median surface displacement vector due to rth modal vibration of the structure that is obtained by IGAFEM procedure.

In this study, it is assumed that the structure oscillates at relatively high frequencies, so that the effect of free surface waves due to the modal vibrations of the structure can be neglected. In this way, the free surface boundary condition can be approximated by the infinite frequency limit condition (Ergin and Uğurlu, 2003),

$$\phi_r = 0. \tag{20}$$

In order to satisfy the condition defined above, the method of images is adopted. The implementation of this method is based on satisfying the zero potential free surface condition by an image body, symmetrically disposed on the opposite side of the free surface. Thus, the problem is reduced to a classical Neumann's case.

3.2.1. Numerical evaluation of perturbation potential ϕ

The boundary integral equation for perturbation potential ϕ can be written as follows

$$c\,\phi(P) = \int_{S_w} q(Q)\,\phi^*(P,Q)\,d\Gamma(Q) - \int_{S_w} \phi(Q)\,q^*(P,Q)\,d\Gamma(Q) \tag{21}$$

where Q and P define the field and evaluation points on the wetted surface, respectively. $q(Q)$ and S_w define the flux and total fluid-structure interaction area of the structure, respectively. $\phi^*(P,Q)$ which is a fundamental solution of the Laplace's equation everywhere except the evaluation point, defines a

potential at the point Q due to unit point source at P and can be defined as

$$\phi^*(P,Q) = \frac{1}{4\pi r}, \tag{22}$$

for the three-dimensional case where

$$r = \sqrt{(x_Q - x_P)^2 + (y_Q - y_P)^2 + (z_Q - z_P)^2} \tag{23}$$

is the distance between the source and field points. Moreover, $q^*(P,Q)$ is the surface normal derivative of the fundamental solution, ϕ^*, and its components in the cartesian coordinate system are expressed as follows

$$q_x^* = \frac{-r_{,x}}{4\pi r^2}, \quad q_y^* = \frac{-r_{,y}}{4\pi r^2}, \quad q_z^* = \frac{-r_{,z}}{4\pi r^2} \tag{24}$$

where

$$r_{,x} = \frac{x_Q - x_P}{r}, \quad r_{,y} = \frac{y_Q - y_P}{r}, \quad r_{,z} = \frac{z_Q - z_P}{r}. \tag{25}$$

Here, Eq. (21) is the Fredholm integral equation of the second kind and it must be satisfied over the wetted and imaginary surfaces of the body. Eq. (21) can be numerically solved by discretizing the wetted and imaginary surfaces of the structure over which the velocity potential and flux is approximated by control point values and the corresponding non-zero rational basis functions at each element as follows

$$\phi^e = \sum_{i=1}^{p+1} \sum_{j=1}^{q+1} R_{i,j}^e \phi_{i,j}^e, \tag{26}$$

$$q^e = \sum_{i=1}^{p+1} \sum_{j=1}^{q+1} R_{i,j}^e q_{i,j}^e. \tag{27}$$

Then, by substituting Eqs. (26) and (27) into Eq. (21) and applying the kinematic boundary condition, the surface integral equation can be written in dis-

cretized form for each principal mode as follows

$$c_k\phi_k^{(r)} + \sum_{e=1}^{n_p}\sum_{i=1}^{p+1}\sum_{j=1}^{q+1}\int_{S^e_{w+i}} R^e_{i,j}\,\phi^{e(r)}_{i,j}\; q^*(P,Q)\,d\Gamma(Q)$$
$$= \sum_{e=1}^{n_p}\sum_{i=1}^{p+1}\sum_{j=1}^{q+1}(\mathbf{u}_{r,ij}\cdot\mathbf{n}_{r,ij})\int_{S^e_{w+i}} R^e_{i,j}\phi^*(P,Q)\,d\Gamma(Q), \quad k=1,...,n_{cp}, \tag{28}$$

where n_p is the total number of hydrodynamic panels (boundary elements), n_{cp} denotes the total number of control points over the discretized surface. S^e_{w+i} represents the surface of the eth hydrodynamic panel on the wetted and imaginary surface of the structure. $\mathbf{u}_{r,ij}$ and $\mathbf{n}_{r,ij}$ denote the modal displacement vector and the surface normal at corresponding control points, respectively. The superscript r figures the sequence of the considered principal modes.

3.2.2. Generalized fluid-structure interaction forces

The kth component of the generalized fluid-interaction forces due to rth modal vibration of the structure can be expressed in terms of the pressure acting on the wetted surface of the structure as follows

$$\bar{Z}_{rk} = \int_{S_w} \mathbf{n}\cdot\mathbf{u}_r\,\bar{P}_k\,d\Gamma. \tag{29}$$

where $\bar{P}_k$ is the fluid pressure acting on the wetted surface and it can be expressed by neglecting the second order terms in the Bernoulli's equation

$$\bar{P}_k = -\rho\frac{\partial\Phi_k}{\partial t}. \tag{30}$$

By substituting Eq. (18) into the above equation, one obtains the fluid pressure acting on the wetted surface of the elastic structure in terms of velocity potential

$$\bar{P}_k = \omega^2\rho\,\Phi_k. \tag{31}$$

By using the harmonic pressure force given Eq. (31) into the Eq. (29), the fluid force acting on the wet surface of the structure is expressed in terms of the

velocity potential

$$\bar{Z}_{rk} = \int_{S_w} \mathbf{n} \cdot \mathbf{u}_r \left(\omega^2 \rho \Phi_k\right) \, d\Gamma, \tag{32}$$

and the generalized added mass term, A_{rk}, can be expressed as follows

$$A_{rk} = \frac{\rho}{\omega^2} \int_{S_w} \mathbf{n} \cdot \mathbf{u}_r \, \omega^2 \Phi_k \, d\Gamma. \tag{33}$$

It is clear that the generalized added mass matrix will be in M-by-M dimension, representing the maximum number of vibration modes considered in the fluid-structure interaction problem. Finally, the discretized form of the generalized added mass term can be rewritten as follows

$$A_{rk} = \frac{\rho}{\omega^2} \sum_{e=1}^{n_p} \sum_{i=1}^{p+1} \sum_{j=1}^{q+1} \int_{S_w^e} R_{i,j}^e \, \phi_{s,ij}^{e^{(r)}} \left(\mathbf{u}_{r,ij} \cdot \mathbf{n}_{r,ij}\right) \, d\Gamma. \tag{34}$$

Therefore, the generalized fluid-structure interaction force, Z_{rk}, is given as

$$Z_{rk} = A_{rk} \omega^2 p_r e^{i\omega t} = -A_{rk} p_r. \tag{35}$$

195 *3.2.3. Calculation of wet frequencies and mode shapes*

For the structure vibrates nearly the free surface or in case where it is partially submerged, the existence of the free surface is significantly alter the fluid effects (added mass and damping) on the structure in the low frequency region. As the frequency increases, the generalized added mass terms tend to decrease and converge to a specific value, while the hydrodynamic damping and stiffness tend to be zero. For the plate considered in this study, it has been observed that the characteristic frequencies obtained from the in-vacuo analysis are in relatively high-frequency region, hence in this case, the generalized added mass terms are independent from the frequency. Therefore, the generalized equation of motion for the fluid-structure interaction system can be expressed as follows

$$\left[-\omega^2 \left(\mathbf{a} + \mathbf{A}\right) + \mathbf{c}\right] = 0 \tag{36}$$

where $\mathbf{a}$ and $\mathbf{c}$ denote the generalized structural mass and stiffness matrices, respectively. The M-by-M $\mathbf{A}$ matrix is formed by the infinite frequency generalized added-mass terms.

By solving the eigenvalue problem expressed in Eq. (36), one can obtain the wet frequencies and associated wet mode shapes of the structure in contact with fluid. For each eigenfrequency, ω_r, there is a corresponding eigenvector $\mathbf{p}_{0r} = [p_{r1}, p_{r2}, ..., p_{rM}]$. The corresponding wet mode shapes for a structure in contact with fluid can be written as

$$\mathbf{q}_r(x, y, z) = \{\bar{u}_r, \bar{v}_r, \bar{w}_r\} = \sum_{j=1}^{M} \mathbf{u}_j(x, y, z)\, \mathbf{p}_{rj} \tag{37}$$

where M denotes the number of modes considered in the analysis and $\mathbf{q}_r(x, y, z)$ represents the shape of the each wet mode in modal space. It should be noted that the fluid-structure interaction forces associated with the inertial effect of the fluid may not have the same spatial distribution as those of the in-vacuo modal forms. As a consequence, this situation points hydrodynamic coupling between the in-vacuo modes. This coupling effect is introduced into Eq. (36) through the generalized added-mass matrix $\mathbf{A}$.

4. IGAFEM/IGABEM Implementation

In order to calculate the hydroelastic vibration characteristics of plates partially or fully immersed into fluid, the flowchart given in Fig. 4 is followed for both in-vacuo and wet analyses in the context of isogemetric approach. In our numerical framework, the geometry is first created, and then following the simple CAD - FEM integration given by Yildizdag (2014), IGA input files which essentially include the geometry data are generated and read by main IGA codes. Then, in-vacuo dynamic characteristics (in-vacuo natural frequencies and mode shapes) of the plate is obtained by solving Eq. (10) as formulated in Section 3. Next, in order to calculate the generalized added-mass terms, the wet analysis is conducted by solving IGABEM formulation in conjuction with the image method as explained in Section 3, and the wet natural frequencies and mode shapes are obtained by solving the eigenvalue problem given in Eq. (36).

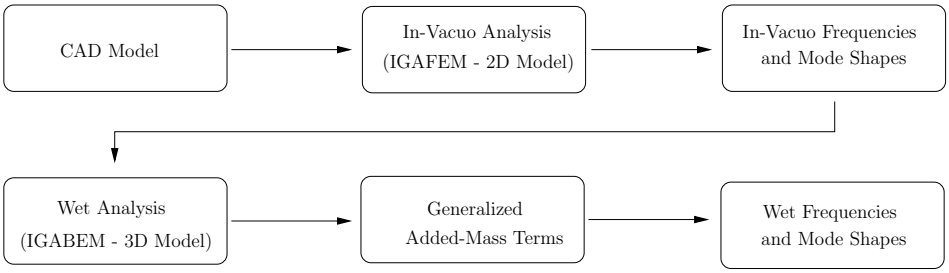

Figure 4: Flowchart for calculating hydroelastic vibration characteristics

Importantly, it must be noticed that different computational domains are used for in-vacuo and wet analyses (see Fig. 5). In-vacuo analysis requires a 2-D mesh (single NURBS patch) to solve the free vibration problem. However, in the wet analysis, thickness of the plate has to be included as both sides of the plate have fluid-structure interface. Thus, six NURBS patches are used to represent the computational domain of the wetted area in the wet analysis.

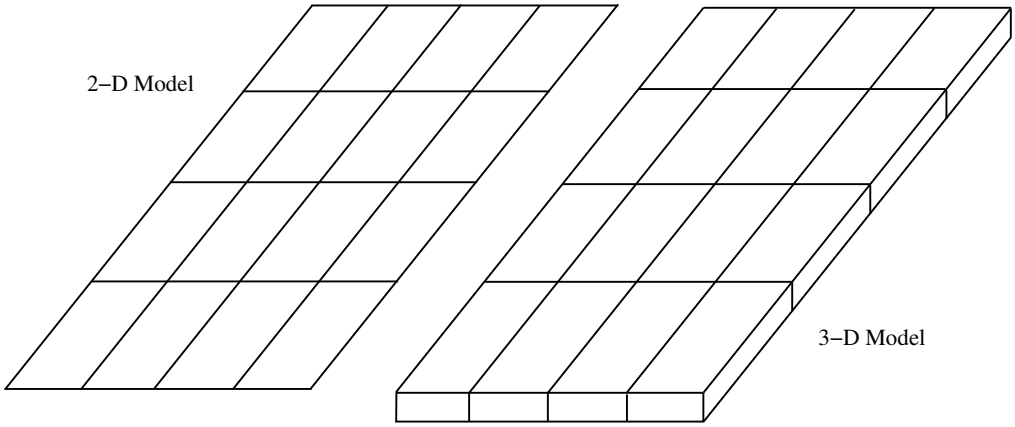

Figure 5: Comparison of computational domains (IGAFEM vs. IGABEM)

In this study, as the plate geometry is represented by flat NURBS surfaces, control points lie on the NURBS surfaces, and their locations are assigned as collocation points for IGABEM procedure. Alternatively, one can determine Greville abscissae (for example, see Simpson et al. (2012)) to assign collocation points if the control points do not lie on the surface of the domain.

5. Numerical Results and Comparisons

In this section, hydroelastic vibration characteristics of plates partially and fully submerged into fluid is studied and calculations have been performed in order to demonstrate the applicability of the aforementioned numerical procedure.

5.1. Cantilever plate vertically in contact with fluid

In the first numerical example, a cantilever plate experimentally studied by Lindholm et al. (1965) was adopted to conduct the numerical study. The plate has length $a = 1.016$ m, width $b = 0.2032$ m, thickness $t = 4.84$ mm (see Fig. 6), and it is made of steel with the following material characteristics: Young's Modulus, $E = 206.8$ GPa, Poisson's Ratio, $\nu = 0.3$, and density, $\rho = 7830$ kg/m^3. Also, the fresh water is used as surrounding fluid with density, $\rho_f = 1000$ kg/m^3. In order to represent the computational domains as explained in Section 4, 2nd-order NURBS patches were used throughout the numerical simulations.

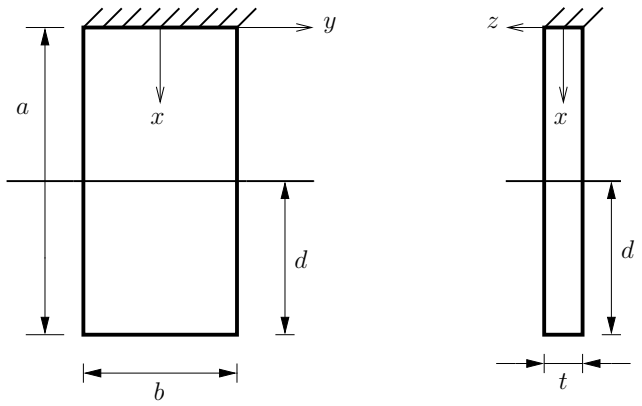

Figure 6: Geometry of the cantilever plate vertically in contact with fluid

5.1.1. In-vacuo analysis

In-vacuo natural frequencies and mode shapes were obtained by solving the free vibration problem formulated for the Kirchhoff plate theory (see Section

3) via IGAFEM procedure. The computational domain was represented by a 2nd-order NURBS patch with 1024 elements (64 elements along the length and 16 elements along the width of the plate) taking into account the convergence study done by Ergin and Uğurlu (2003) for the same problem.

Mode No	Mode Shape	IGAFEM (1024 Elements)	FEM (1024 Elements)	Kwak and Yang (2013)	Lindholm et al. (1965)
1	S	3.94	3.95	3.98	3.84
2	S	24.69	24.72	24.91	24.20
3	A	39.37	39.13	39.55	39.10
4	S	69.32	69.33	69.84	68.10
5	A	120.44	119.71	121.05	121.00
6	S	136.39	136.28	137.35	-

Table 1: In-vacuo frequencies (Hz)

In order to verify the calculated results and have a better comparison, the same problem was also solved by a standard finite element software, ANSYS®. The same mesh structure (1024 elements with 2nd-order finite elements) were adopted in standard FEM solution. In Table 1, the calculated in-vacuo frequencies by IGAFEM are compared with FEM, semi-analytical, and experimental results, for the first six modes. Also, corresponding in-vacuo mode shapes are depicted in Fig. 7, for the first six modes. Here, the mode shapes can be divided into two groups due their displacement characteristics: symmetric (S) and antisymmetric (A). The displacement characteristics of a symmetric mode shape has symmetry about x-axis while an antisymmetric mode shape has the opposite characteristics. As seen in Table 1, IGAFEM results show excellent agreement with standard FEM, semi-analytical, and experimental results.

5.1.2. Wet analysis

A series of calculations were performed by using IGABEM procedure to test the convergence of the hydrodynamic properties of the cantilever plate. The numerical tests were carried out separately for four different depth ratios, namely $d/a = 0.25, 0.5, 0.75$, and 1. In the convergence study, each test case was identified by the number of panels (boundary elements) along the width of

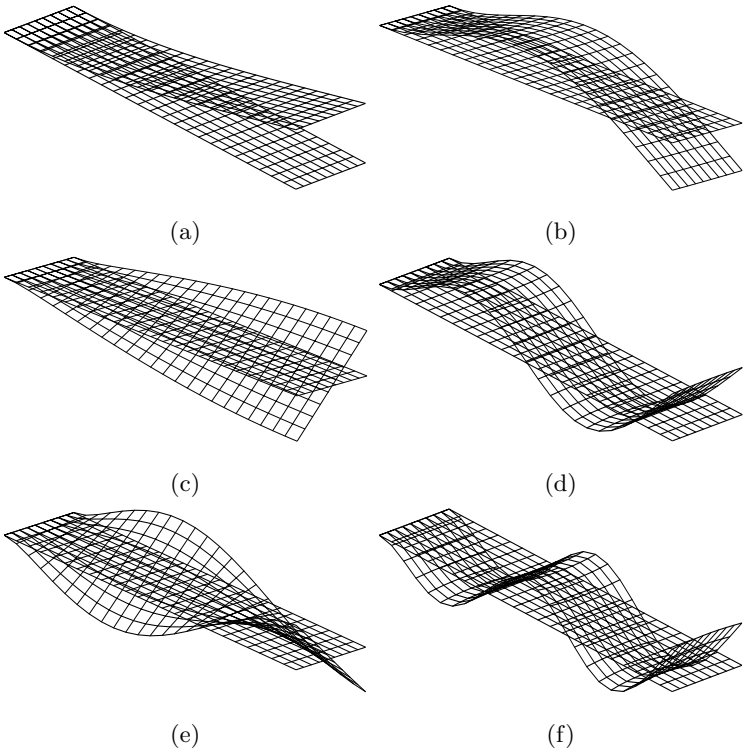

Figure 7: In-vacuo mode shapes of cantilever plate (IGAFEM results): (a) 1st mode (3.94 Hz); (b) 2nd mode (24.69 Hz); (c) 3rd mode (39.37 Hz); (d) 4th mode (69.32 Hz); (e) 5th mode (120.44 Hz); (f) 6th mode (136.39 Hz)

the plate, and the aspect ratio (a/b) of the panels on top and bottom surfaces of the plate was taken same in each test.

In the first group of calculations, NURBS patches with the total discretization of 44, 84, 124, and 164 panels were used for the depth ratios $d/a = 0.25$, 0.5, 0.75, and 1, respectively. The number of elements along the width was 4 for each depth ratio while the number of elements along the length of the wetted plate was 4, 8, 12, and 16, respectively. After that number of panels was increased to 90, 174, 258, and 342 for the second group of calculations, with 6 elements along the width and 6, 12, 18, and 24 elements along the length of the wetted plate, respectively, for the depth ratios $d/a = 0.25$, 0.5, 0.75, and 1. Subsequently, the number of panels was increased to 152, 174, 440, and 584, and finally to 230, 450, 670, and 890 for $d/a = 0.25, 0.5, 0.75$, and 1, respectively. The number of panels along the width was 8 for the third group, and 10 for the fourth group of calculations. Additionally, another convergence study was carried out to determine the number of modes needed for the calculations. As a result of this additional analysis, 12 in-vacuo modes were included in the calculations.

The predicted wet natural frequencies are presented in Table 7 for $d/a = 0.25$ and 0.5, and in Table 3 for $d/a = 0.75$ and 1. The differences between the last two groups are reasonably small for all different depth ratios and therefore, it may be said that the final group of calculations (230, 450, 670, and 890 panels) adequately represents the hydroelastic vibration characteristics of the cantilever plate. The calculated results are compared with the experimental results in Table 4. The calculated wet frequencies show very good agreement with the experimental data and it is observed that the differences are in the range of 0.2%-6%. The highest relative error (5.77%) in wet frequencies has been observed in the fourth mode of the depth ratio 0.25.

Mode No	Mode Shape	Depth Ratio (d/a)							
		0.25				0.5			
		44 Panels	90 Panels	152 Panels	230 Panels	84 Panels	174 Panels	296 Panels	450 Panels
1	S	2.34	2.30	2.29	2.29	1.78	1.81	1.84	1.86
2	S	21.40	21.41	21.42	21.42	17.08	16.34	16.08	15.98
3	A	30.88	29.97	29.67	29.42	26.15	25.34	25.16	25.16
4	S	62.75	61.69	61.06	60.67	54.90	53.56	53.03	52.80
5	A	106.13	105.46	105.30	105.25	99.80	96.62	95.34	94.87
6	S	123.68	120.39	118.79	117.93	112.06	105.34	102.29	100.84

Table 2: Convergence of wet natural frequencies (Hz) for depth ratios 0.25 and 0.5

Mode No	Mode Shape	Depth Ratio (d/a)							
		0.75				1.0			
		124 Panels	258 Panels	440 Panels	670 Panels	164 Panels	342 Panels	584 Panels	890 Panels
1	S	1.68	1.72	1.75	1.77	1.66	1.71	1.74	1.76
2	S	12.53	12.18	12.11	12.11	11.46	11.36	11.40	11.45
3	A	24.92	24.09	23.86	23.85	24.64	23.85	23.65	23.64
4	S	44.23	41.19	39.99	39.48	36.76	34.88	34.29	34.12
5	A	83.13	79.14	77.73	77.30	77.70	74.35	72.96	71.82
6	S	100.92	93.14	89.46	87.65	82.70	75.66	73.32	73.10

Table 3: Convergence of wet natural frequencies (Hz) for depth ratios 0.75 and 1.0

Moreover, Table 5 compares the predicted wet frequencies with the results presented by Ergin and Uğurlu (2003) and Kwak and Yang (2013). Importantly, it can be seen that less number of panels is required for the convergence compared with the study presented by Ergin and Uğurlu (2003) which uses the same methodology with the conventional BEM procedure (with constant boundary elements). In their study, the convergence of the wet frequencies has been obtained with 320, 608, 896, and 1184 panels, respectively, for the depth ratios $d/a = 0.25$, 0.5, 0.75, and 1.

Mode No	Mode Shape	This study					Lindholm et al. (1965)				
		In vacuo	Depth Ratio (d/a)				In air	Depth Ratio (d/a)			
			0.25	0.5	0.75	1.0		0.25	0.5	0.75	1.0
1	S	3.94	2.29	1.86	1.77	1.76	3.84	2.17	1.82	1.79	1.78
2	S	24.69	21.42	15.98	12.11	11.45	24.20	21.01	15.50	11.99	11.50
3	A	39.37	29.42	25.16	23.85	23.64	39.10	29.75	25.50	24.20	24.20
4	S	69.32	60.67	52.80	39.48	34.12	68.10	57.36	51.61	38.27	33.50
5	A	120.44	105.25	94.87	77.30	71.82	121.00	106.35	95.99	79.00	75.26
6	S	136.39	117.93	100.84	87.65	73.10	-	-	-	-	-

Table 4: Comparison with the experimental results

It can be seen from Tables 4 and 5 that the wet frequencies behave as expected, and they decrease with increasing area of fluid contact. Therefore, the lowest frequency values have been obtained for the depth ratio $d/a = 1$.

Mode No	Mode Shape	This study				Ergin and Uğurlu (2003)				Kwak and Yang (2013)			
		Depth Ratio (d/a)				Depth Ratio (d/a)				Depth Ratio (d/a)			
		0.25	0.5	0.75	1.0	0.25	0.5	0.75	1.0	0.25	0.5	0.75	1.0
1	S	2.29	1.86	1.77	1.76	2.29	1.90	1.83	1.82	2.46	1.89	1.78	1.77
2	S	21.42	15.98	12.11	11.45	21.32	15.69	12.20	11.68	20.37	16.00	12.55	11.56
3	A	29.42	25.16	23.85	23.64	29.42	25.43	24.16	24.00	31.11	26.53	25.04	24.67
4	S	60.67	52.80	39.48	34.12	59.32	52.23	38.67	34.31	59.81	49.81	40.50	34.07
5	A	105.25	94.87	77.30	71.82	105.01	93.84	77.31	73.91	106.97	95.00	80.66	70.53
6	S	117.93	100.84	87.65	73.10	116.64	98.71	84.46	71.22	119.05	101.95	85.75	75.85

Table 5: Comparison with the numerical and semi-analytical results

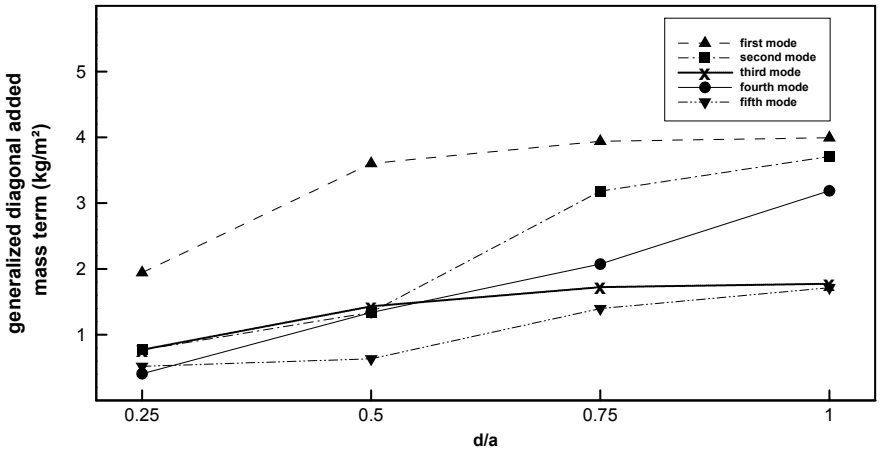

Figure 8: Generalized diagonal added mass terms for the first five mode

The generalized diagonal added mass terms for first 5 distortional modes for the depth ratios d/a= 0.25, 0.5, 0.75, 1 are shown in Fig. 8 and they correspond to a generalized structural mass of 1 kg m^2. In order to calculate the generalized added mass terms, pressure distribution over the wet part of the structure is obtained on the assumption that the structure vibrates in its vacuo principal mode shapes in the fluid. As seen from Fig. 8, the generalized diagonal added mass terms become larger as the total wet surface area of the plate increases.

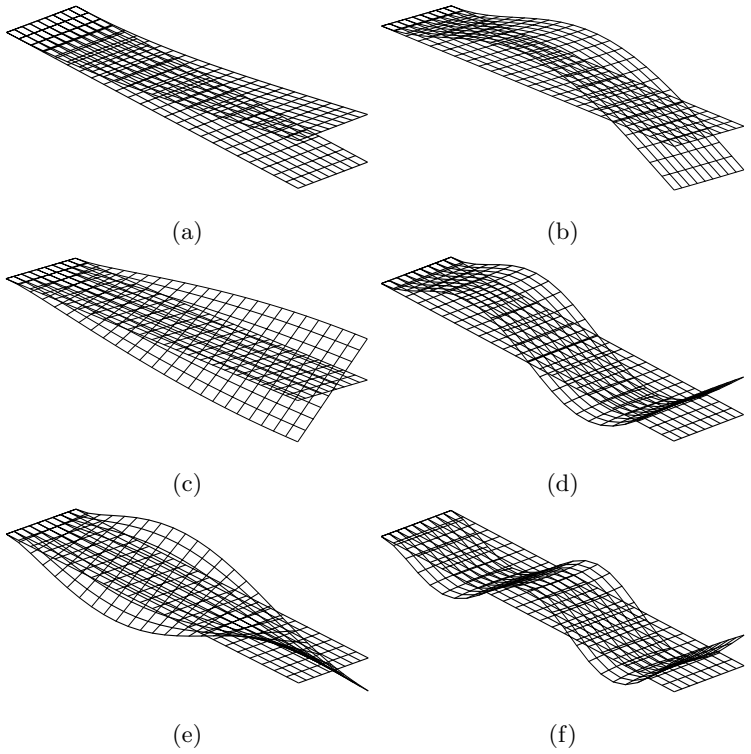

Figure 9: Wet mode shapes of cantilever plate for depth ratio d/a=0.5: (a) 1st mode (1.86 Hz); (b) 2nd mode (15.98 Hz); (c) 3rd mode (25.16 Hz); (d) 4th mode (52.80 Hz); (e) 5th mode (105.25 Hz); (f) 6th mode (120.39 Hz)

315 The generalized added mass coefficients corresponding to the first 6 in-vacuo modes, 4 symmetric (S) and 2 antisymmetric (A), are compared with the results given by Ergin and Uğurlu (2003) in Table 6 for the submergence rate $d/a = 0.5$. The generalized added mass coefficients are calculated under the assumption that the rectangular plate is vibrating in-vacuo mode shapes when 320 it has contact with fluid; thereby, each mode has unique surface pressure distribution related to its in-vacuo modal configuration. Following that, the generalized added mass coefficients were calculated by utilizing Eq. (34) over the wetted part of the structure. It is observed from Table 6 that the diagonal elements of the generalized added mass matrix are considerably larger that the 325 non-diagonal ones, which stand for the hydrodynamic interaction between the

in-vacuo modes of the structure, in related row and column. This situation also clarifies the negligible difference between the in-vacuo and wet mode shapes of the plate (see Fig. 7 and Fig. 9). Additionally, the symmetrical formation of the generalized added mass matrix emphasizes the reciprocal characteristic of the problem, which indicates that the hydrodynamic coupling effects of the mutual modes on each other are the same. As the mode number increases, in other words, as the number of stationary points increases in the modal configuration of the structure, the generalized added mass coefficients for the respective mode are reduced. Furthermore, the hydrodynamic interaction between the symmetric and antisymmetric modes seems to be quite strong in itself compared to the interaction with the modes in opposing group.

Mode No	Mode Shape	This study						Mode No	Mode Shape	Ergin and Uğurlu (2003)					
1	S	3.368	0.380	0.000	0.735	0.000	0.510	1	S	3.301	0.316	0.001	0.719	0.001	0.440
2	S	0.380	1.361	0.000	1.030	0.000	0.004	2	S	0.316	1.424	0.002	1.019	0.002	0.086
3	A	0.000	0.000	1.396	0.000	0.516	0.000	3	A	0.001	0.002	1.349	0.000	0.472	0.000
4	S	0.735	1.030	0.000	1.364	0.000	0.644	4	S	0.719	1.019	0.000	1.337	0.001	0.602
5	A	0.000	0.000	0.516	0.000	0.630	0.000	5	A	0.001	0.002	0.472	0.001	0.630	0.000
6	S	0.510	0.004	0.000	0.644	0.000	1.027	6	S	0.440	0.086	0.000	0.602	0.000	1.074

Table 6: Comparison of generalized added mass values

In addition, another convergence study was conducted to determine the number of hydrodynamic panels needed to obtain the generalized added mass values, and the results are given in Fig. 10 for the first three diagonal added mass terms for different submergence ratios. As can be seen from Fig. 10, the difference between the generalized added mass values become negligibly small for the third and fourth discretization levels for all submergence ratios, and all the added mass values converge monotonically.

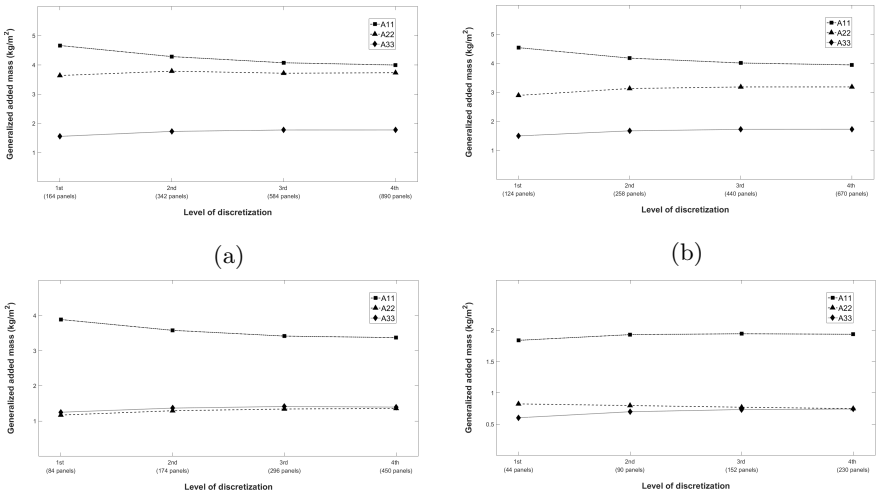

Figure 10: Convergence of the generalized added mass coefficients

Later, the numerical study was extended to investigate the effects of the plate aspect ratio (a/b) and thickness ratio (t/b) on the hydroelastic vibration characteristics. Fig. 11 shows the predicted wet natural frequencies for five different aspect ratios, $a/b = 1$, 2, 3, 4, and 5, with using three different thickness ratios, $t/b = 0.0238$, 0.0476, and 0.0714, for the first six modes and depth ratio 0.5. In the calculations the width (b) of the plate was kept constant, and the length (a) and the thickness (t) were changed for different values of aspect and thickness ratios. It is clear that wet natural frequencies increase with increasing thickness ratio, and decrease with increasing aspect ratio.

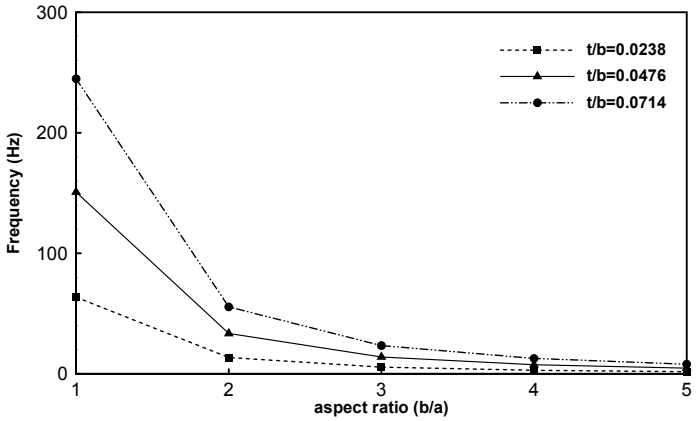

(a) 1st mode

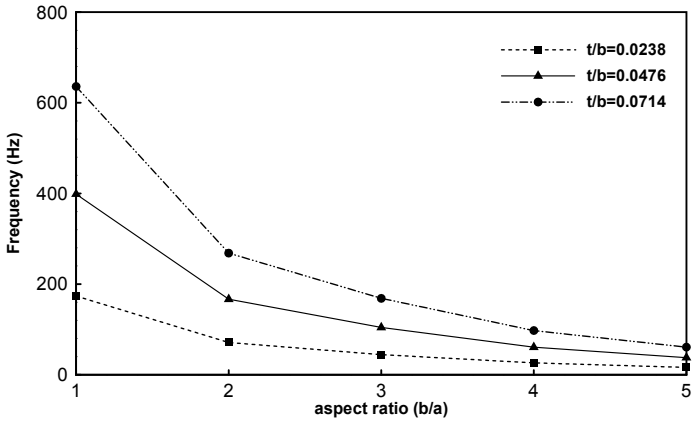

(b) 2nd mode

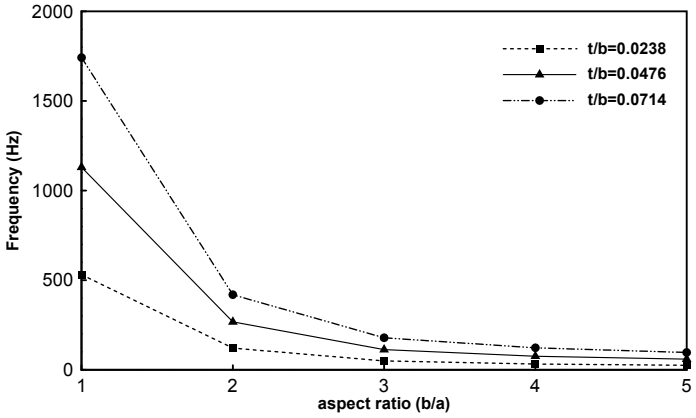

(c) 3rd mode

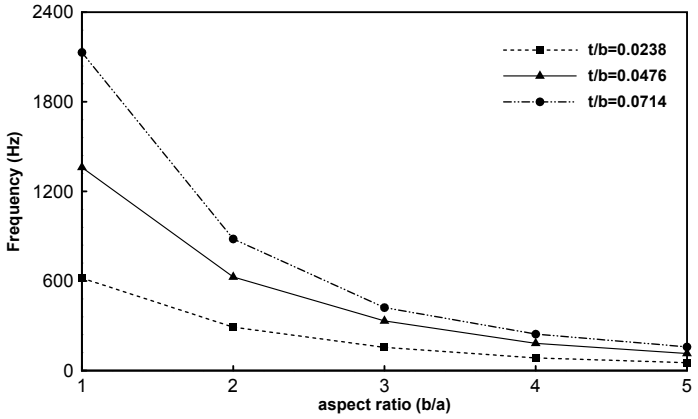

(d) 4th mode

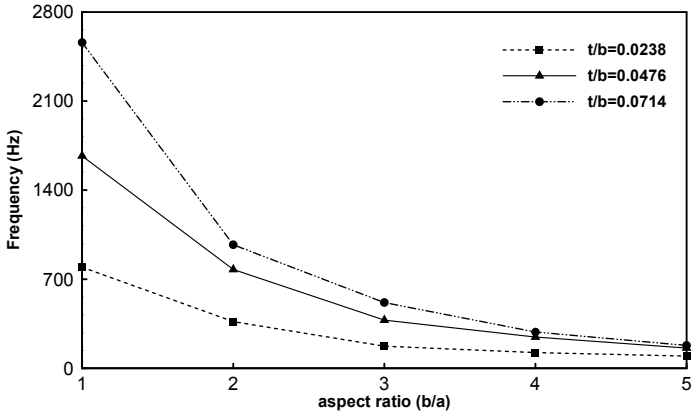

(e) 5th mode

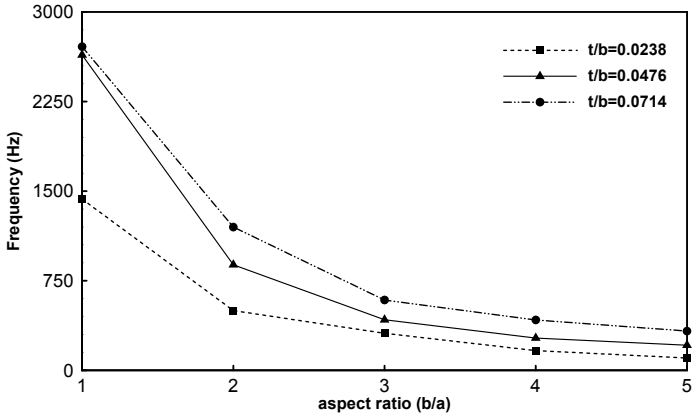

(f) 6th mode

Figure 11: Wet frequencies for different t/b values and depth ratio $d/a = 0.5$

5.2. Cantilever plate horizontally in contact with fluid

In a further study, the results obtained for the partially submerged vertical cantilever plate in the previous section are expanded to the case where the cantilever plate is in a horizontal position within the fluid environment. In this case, the cantilever plate is totally submerged near the free surface of the fluid (see Fig. 12). This type of hydroelastic vibration problem have been investigated experimentally (Lindholm et al., 1965) and numerically (Fu and Price, 1987) by several authors. The geometric properties of the plate are: $a = b = 10$ m, and the thickness $t = 0.238$ m. The mechanical properties of the plate are: Young's modulus $E = 206.8$ GPa, material density $\rho = 7830\,\mathrm{kg/m^3}$, and the Poisson's ratio $\nu = 0.3$. In this examination, it is assumed that the horizontal cantilever plate is placed into unbounded fluid medium, in the absence of any rigid wall effects. The same approach in the previous section is followed, the infinite frequency limit on the free surface is adopted by the image method and fluid-structure coupling effects are represented by generalized added mass matrix in the equation of motion.

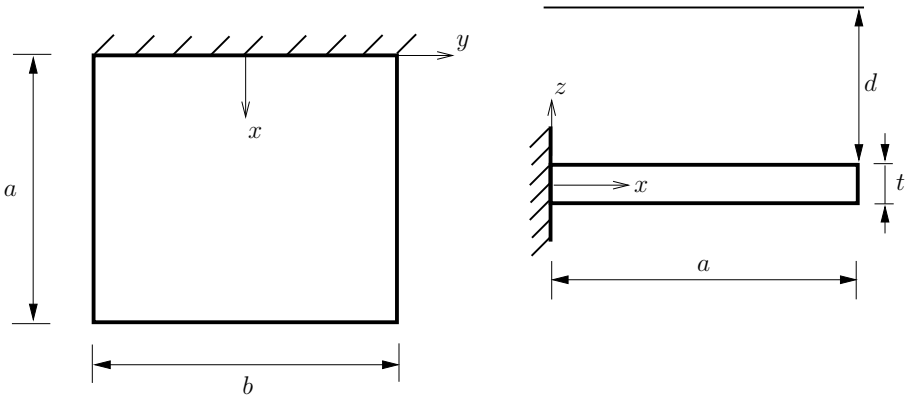

Figure 12: Geometry of the cantilever plate horizontally in contact with fluid

The numerical studies are performed for four different depth ratios, namely $d/a = 0.05, 0.1, 0.3$, and 0.5, and additionally, the case where the cantilever plate is infinitely submerged is also included into the series of calculations. The domain was discretized along both in-plane directions with 16 equally-spaced

quadrilateral elements, and they correspond to a total 256 elements for the in-vacuo analysis. On the other hand, 576 quadrilateral panels (512 panels on both sides of the plate and 64 panels along the thickness) were used to conduct the wet analysis. The first six wet frequencies for different d/a ratios are listed in Table 8 and compared with the numerical results provided by Fu and Price (1987) and Kerboua et al. (2008). The discrepancies between the predicted results in this study and the results obtained in Fu and Price (1987) are negligibly small due to adopting the boundary element method in the calculation of the effects of the fluid on the structure in both studies. The differences between these studies lie between 0.1% and 4.1%.

Mode No	Mode Shape	Depth Ratio (d/a)											
		0.05			0.1			0.3			0.5		
		160 Panels	240 Panels	336 Panels	160 Panels	240 Panels	336 Panels	160 Panels	240 Panels	336 Panels	160 Panels	240 Panels	336 Panels
1	S	1.29	1.30	1.31	1.23	1.24	1.25	1.14	1.15	1.16	1.12	1.13	1.14
2	S	3.52	3.53	3.54	3.38	3.38	3.39	3.19	3.20	3.21	3.16	3.17	3.19
3	A	9.03	8.94	8.90	8.70	8.60	8.55	8.26	8.14	8.08	8.17	8.05	7.99
4	S	11.71	11.56	11.48	11.35	11.19	11.11	11.00	10.82	10.72	10.97	10.78	10.69
5	A	13.85	13.69	13.63	13.37	13.20	13.12	12.87	12.68	12.60	12.82	12.63	12.54
6	S	24.48	24.07	23.84	23.87	23.39	23.13	23.38	22.85	22.56	23.36	22.83	22.53

Table 7: Convergence of wet natural frequencies (Hz) for horizontal cantilever plate

Mode No	Mode Shape	This study Depth Ratio (d/a)				Fu and Price (1987) (240 Panels) Depth Ratio (d/a)				Kerboua et al. (2008) Depth Ratio (d/a)			
		0.05	0.1	0.3	0.5	0.05	0.1	0.3	0.5	0.05	0.1	0.3	0.5
1	S	1.32	1.26	1.17	1.15	1.42	1.28	1.20	1.17	1.37	1.30	1.18	1.11
2	S	3.56	3.42	3.24	3.21	3.68	3.43	3.24	3.21	3.36	3.19	2.89	2.73
3	A	8.83	8.47	7.99	7.90	8.86	8.47	8.09	7.98	8.42	8.01	7.26	6.84
4	S	11.43	11.05	10.65	10.61	12.03	11.49	11.27	11.06	-	-	-	-
5	A	13.58	13.06	12.51	12.46	13.60	12.99	12.47	12.35	-	-	-	-
6	S	23.64	22.89	22.28	22.24	-	-	-	-	-	-	-	-

Table 8: Comparison of wet frequencies (Hz) for horizontal cantilever plate

The generalized diagonal added mass terms for depth ratios $d/a = 0.05$, 0.1, 0.3, 0.5 and also for the infinitely submerged state are shown in Fig. 13. As expected, the generalized diagonal added mass terms become larger as the submergence ratio of the plate increases. It can be said that the difference between the generalized diagonal added mass terms are noticeable until the d/a is equal to 0.3. This difference decreases considerably when the d/a ratio is between 0.3 and 0.5; and further increment of d/a ratio up to 0.5, the generalized diagonal added mass terms are virtually fixed to certain value. In other words, when the depth ratio exceeds 0.5, the generalized diagonal added mass terms are equal to the case where the plate infinitely immersed into fluid medium.

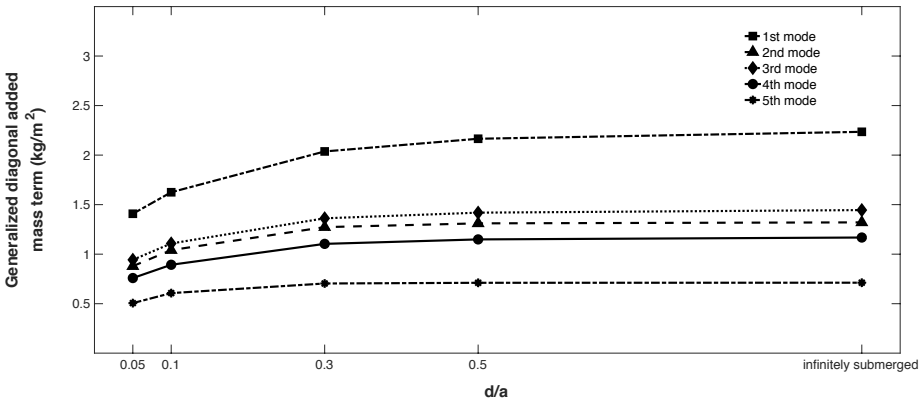

Figure 13: Generalized diagonal added mass terms for the first five mode (horizontal cantilever plate)

6. Conclusions

The hydroelastic vibration characteristics (wet natural frequencies and mode shapes) of cantilever plates was investigated by the proposed numerical procedure in the context of isogeometric approach. In this numerical framework, in-vacuo natural frequencies and mode shapes have been first obtained by solving the free vibration problem with the isogeometric finite element method (IGAFEM). Then, in the second part of the analysis, using in-vacuo vibration characteristics, the generalized added-mass terms have been calculated by isogeometric boundary element method (IGABEM) in conjuction with the image method.

In the first numerical example, a cantilever plate vertically in contact with fluid was considered. The numerical results presented for in-vacuo and wet natural frequencies show very good agreement with the experimental results presented by Lindholm et al. (1965) (see Table 4), and it is observed that the differences are in the acceptable range. On the other hand, the predicted wet frequencies were compared with the numerical and semi-analytical results (see Table 5) given by Ergin and Uğurlu (2003) and Kwak and Yang (2013), respectively. Here, it is also showed that less number of panels is required in the convergence study (see Tables 3 and 7). Then, the calculations were carried out to study the effects of aspect and thickness ratios on the hydrodynamic characteristics of the cantilever plate. Later, a horizontally submerged cantilever plate was considered, and the predicted hydroelastic vibration characteristics were compared with the numerical results (see Table 8) presented by Fu and Price (1987) and Kerboua et al. (2008).

The results presented in this study show that the proposed method is suitable for relatively high-frequency vibrations of partially or fully submerged elastic structures.

Acknowledgements

M. E. Yildizdag gratefully acknowledges the financial support from The Scientific and Technological Research Council of Turkey (TUBITAK), under the programme BIDEB 2213.

References

Bazilevs, Y., Calo, V., Zhang, Y., Hughes, T.J., 2006a. Isogeometric fluid–structure interaction analysis with applications to arterial blood flow. Computational Mechanics 38, 310–322.

Bazilevs, Y., Beirao da Veiga, L., Cottrell, J.A., Hughes, T.J., Sangalli, G., 2006b. Isogeometric analysis: approximation, stability and error estimates for h-refined meshes. Mathematical Models and Methods in Applied Sciences 16, 1031–1090.

Belibassakis, K., Gerostathis, T.P., Kostas, K., Politis, C., Kaklis, P., Ginnis, A., Feurer, C., 2013. A bem-isogeometric method for the ship wave-resistance problem. Ocean Engineering 60, 53–67.

Canales, F., Mantari, J., 2017. Laminated composite plates in contact with a bounded fluid: Free vibration analysis via unified formulation. Composite Structures 162, 374–387.

Cho, D.S., Kim, B.H., Vladimir, N., Choi, T.M., 2014. Natural vibration analysis of vertical rectangular plates and stiffened panels in contact with fluid on one side. Proceedings of the Institution of Mechanical Engineers, Part M: Journal of Engineering for the Maritime Environment 230, 114–125.

Cottrell, J.A., Hughes, T.J., Bazilevs, Y., 2009. Isogeometric analysis: toward integration of CAD and FEA. John Wiley & Sons.

De Luycker, E., Benson, D., Belytschko, T., Bazilevs, Y., Hsu, M., 2011. X-fem in isogeometric analysis for linear fracture mechanics. International Journal for Numerical Methods in Engineering 87, 541–565.

Ergin, A., Uğurlu, B., 2003. Linear vibration analysis of cantilever plates partially submerged in fluid. Journal of Fluids and Structures 17, 927–939.

Fu, Y., Price, W., 1987. Interactions between a partially or totally immersed vibrating cantilever plate and the surrounding fluid. Journal of Sound and Vibration 118, 495–513.

Gong, Y., Dong, C., 2017. An isogeometric boundary element method using adaptive integral method for 3d potential problems. Journal of Computational and Applied Mathematics 319, 141–158.

Hashemi, S.H., Karimi, M., Rokni, H., 2012. Natural frequencies of rectangular mindlin plates coupled with stationary fluid. Applied Mathematical Modelling 36, 764–778.

Hashemi, S.H., Karimi, M., Taher, H.R.D., 2010. Vibration analysis of rectangular mindlin plates on elastic foundations and vertically in contact with stationary fluid by the ritz method. Ocean Engineering 37, 174–185.

Hughes, T.J., Cottrell, J.A., Bazilevs, Y., 2005. Isogeometric analysis: Cad, finite elements, nurbs, exact geometry and mesh refinement. Computer methods in applied mechanics and engineering 194, 4135–4195.

Kerboua, Y., Lakis, A., Thomas, M., Marcouiller, L., 2008. Vibration analysis of rectangular plates coupled with fluid. Applied Mathematical Modelling 32, 2570–2586.

Kwak, M.K., 1996. Hydroelastic vibration of rectangular plates. TRANSACTIONS-AMERICAN SOCIETY OF MECHANICAL ENGINEERS JOURNAL OF APPLIED MECHANICS 63, 110–115.

Kwak, M.K., Yang, D.H., 2013. Free vibration analysis of cantilever plate partially submerged into a fluid. Journal of Fluids and Structures 40, 25–41.

Kwak, M.K., Yang, D.H., 2015. Dynamic modelling and active vibration control of a submerged rectangular plate equipped with piezoelectric sensors and actuators. Journal of Fluids and Structures 54, 848–867.

Li, P.L., Shyu, R.J., Wang, W.H., Cheng, C.Y., 2011. Analysis and reversal of dry and hydroelastic vibration modes of stiffened plates. Ocean Engineering 38, 1014–1026.

Liang, C.C., Liao, C.C., Tai, Y.S., Lai, W.H., 2001. The free vibration analysis of submerged cantilever plates. Ocean Engineering 28, 1225–1245.

Liao, C.Y., Ma, C.C., 2016. Vibration characteristics of rectangular plate in compressible inviscid fluid. Journal of Sound and Vibration 362, 228–251.

Lindholm, U.S., Kana, D.D., Chu, W.H., Abramson, H.N., 1965. Elastic vibration characteristics of cantilever plates in water. Journal of Ship Research 9, 11–22.

Luu, A.T., Kim, N.I., Lee, J., 2015. Nurbs-based isogeometric vibration analysis of generally laminated deep curved beams with variable curvature. Composite Structures 119, 150–165.

Marcus, M.S., 1978. A finite-element method applied to the vibration of submerged plates. Journal of Ship Research 22.

Meyerhoff, W., 1970. Added masses of thin rectangular plates calculated from potential theory. J Ship Res 14, 100–111.

Muthuveerappan, G., Ganesan, N., Veluswami, M., 1979. A note on vibration of a cantilever plate immersed in water. Journal of Sound and Vibration 63, 385–391.

Piegl, L., Tiller, W., 1995. The NURBS book. Springer.

Politis, C., Ginnis, A.I., Kaklis, P.D., Belibassakis, K., Feurer, C., 2009. An isogeometric bem for exterior potential-flow problems in the plane, in: 2009 SIAM/ACM Joint Conference on Geometric and Physical Modeling, ACM. pp. 349–354.

Rogers, D.F., 2000. An introduction to NURBS: with historical perspective. Elsevier.

Shojaee, S., Izadpanah, E., Valizadeh, N., Kiendl, J., 2012. Free vibration analysis of thin plates by using a nurbs-based isogeometric approach. Finite Elements in Analysis and Design 61, 23–34.

Simpson, R.N., Bordas, S.P., Trevelyan, J., Rabczuk, T., 2012. A two-dimensional isogeometric boundary element method for elastostatic analysis. Computer Methods in Applied Mechanics and Engineering 209, 87–100.

Takahashi, T., Matsumoto, T., 2012. An application of fast multipole method to isogeometric boundary element method for laplace equation in two dimensions. Engineering Analysis with Boundary Elements 36, 1766–1775.

Temizer, I., Wriggers, P., Hughes, T., 2011. Contact treatment in isogeometric analysis with nurbs. Computer Methods in Applied Mechanics and Engineering 200, 1100–1112.

Thai, C.H., Nguyen-Xuan, H., Nguyen-Thanh, N., Le, T.H., Nguyen-Thoi, T., Rabczuk, T., 2012. Static, free vibration, and buckling analysis of laminated composite reissner–mindlin plates using nurbs-based isogeometric approach. International Journal for Numerical Methods in Engineering 91, 571–603.

Uğurlu, B., Kutlu, A., Ergin, A., Omurtag, M., 2008. Dynamics of a rectangular plate resting on an elastic foundation and partially in contact with a quiescent fluid. Journal of sound and Vibration 317, 308–328.

Wang, D., Liu, W., Zhang, H., 2015. Superconvergent isogeometric free vibration analysis of euler–bernoulli beams and kirchhoff plates with new higher order mass matrices. Computer Methods in Applied Mechanics and Engineering 286, 230–267.

Yildizdag, M.E., 2014. Isogeometric Structural Analysis of Beams and Plates. Master's thesis. Istanbul Technical University.

Yoon, M., Cho, S., 2016. Isogeometric shape design sensitivity analysis of elasticity problems using boundary integral equations. Engineering Analysis with Boundary Elements 66, 119–128.

Zhang, Y., Bazilevs, Y., Goswami, S., Bajaj, C.L., Hughes, T.J., 2007. Patient-specific vascular nurbs modeling for isogeometric analysis of blood flow. Computer methods in applied mechanics and engineering 196, 2943–2959.

Zhao, G., Du, X., Wang, W., Liu, B., Fang, H., 2017. Application of isogeometric method to free vibration of reissner–mindlin plates with non-conforming multi-patch. Computer-Aided Design 82, 127–139.

Zhou, D., Cheung, Y., 2000. Vibration of vertical rectangular plate in contact with water on one side. Earthquake engineering & structural dynamics 29, 693–710.

Zienkiewicz, O., Newton, R., 1969. Coupled vibrations of a structure submerged in a compressible fluid, in: Symposium on Finite Element Techniques. Germany: Univ. of Stuttgart.